Rapid turning maneuver flight control for a high agility UAV using robust adaptive augmented backstepping*

Yi Yang, Xin Chen, and Chuntao Li

Abstract—**The paper presents a new robust adaptive augmented backstepping control scheme for rapid turning maneuver of a high agility unmanned aerial vehicle (UAV). The proposed control scheme consists of a baseline backstepping controller which can deal with the couplings of kinematic and inertial during fast rolling and generates commands tracking control inputs, and a robust adaptive compensator which can ensure bounded output tracking error in the presence of unmodeled dynamics. Effectiveness and robustness of the designed scheme has been verified through detailed stability analysis and a number of simulations on a nonlinear 6DOF UAV model which show that the proposed robust adaptive augmented controller is competent to perform rapid turning maneuver in full flight envelop and improve the robustness of flight control system substantially.**

I. INTRODUCTION

The rapid turning maneuver is an aggressive lateral maneuver for an UAV as shown in Fig.1. In this maneuver, the UAV turns continuously with smaller turning radius and holds the altitude at a constant meanwhile. In the military aerospace community, the potential benefits of rapid turning maneuver flight are attractive [1]. For example, an UAV with rapid turning maneuver capability can be customized for specific missions such as evading attack, formation flying and fast tail chasing, which meanwhile greatly improve the survival probability and versatility of UVA as a kind of conventional weapons in battlefield scenarios.

Plenty of investigations concerning maneuver flight control have been presented. The X-31 program, borne in the cold-war era, was proposed to demonstrate the feasibility of exploiting several advanced vehicle control and related technologies to provide greatly enhanced maneuver ability (see [2]). In [3], a linear PID controller with scheduled gain is designed for an indoor autonomous vehicle to perform transition from level-flight to hover maneuver at MIT. Whereas the linearization method is limited to perform in nonlinear regime, multiple controllers are needed to be designed independently in different flight envelope regions and such process requires numerous Monte Carlo simulations, the cost of which grows with the increasing complexity of the system. The use of nonlinear controllers provides means of control at all possible regimes. In [4], nonlinear decoupling theory and dynamic inversion approach have been applied to flight control system. Reference [5] presents a dynamic sliding mode controller for a set of decomposed simplified predefined maneuvers.

To handle the unmodeled dynamics, which may have great influence on rapid turning maneuver, several studies make valuable contributions. The author in reference [6] proposed a robust adaptive nonlinear controller design method which provides a useful way to deal with both parameter uncertainty and unknown nonlinearities of the plant with the known knowledge of upper bound of the uncertainties, which is hard to obtain in advance in practice. In [7], B-spline neural networks are used inside the parameter update laws of the backstepping controller to approximate the nonlinear uncertain aerodynamic forces and moments of F-16/MATV aircraft. And the same technology is also found in [8]. Recently, a novel model reference adaptive controller associated with low-pass filter for a class of uncertain nonlinear systems in the presence of unmodeled dynamics is designed to ensure the tracking error uniformly bounded (see [9] and [10]). All of them are intend to enhance robustness of control system.

In this paper, a three-axis nonlinear backstepping control law is developed as a baseline controller which is able to counteract nonlinear interactions and guarantee all the closed-loop system stability. Besides, an observer based robust adaptive compensator is adopted to compensate the aerodynamic uncertainties and disturbance moments which are separated as matched and unmatched uncertain items estimated online. The combination of the backstepping control and the robust adaptive compensator can guarantee that the closed-loop system is stable and the output tracking errors can be made sufficiently small by proper choice of design parameters.

II. PROBLEM STATEMENT AND UAV MODEL

In this Section, we first present kinematic and inertial couplings, then give the UAV dynamic equations to be studied and formulate the rapid turning maneuver control problem.

A. Kinematic and inertial couplings during rapid turning

If the aircraft initiating a body-axis roll from otherwise wings-level flight will kinematically convert angle of attack into sideslip (see Fig.1). Extremely, a body-axis roll of 90° will lead to a complete conversion from angle of attack into sideslip. In reality, since the existence of longitudinal and directional damping moment, the real roll axis p_{real} is between body-axis and velocity vector.

*Resrach supported by Science and Technology on Aircraft Control Laboratory under grant 20125852057. And Funding of Jiangsu Innovation Program for Graduate Education under grants CXLX12_0159 and the Fundamental Research Funds for the Central Universities.

Yi Yang is a doctor candidate in College of Automation Engineering, Nanjing University of Aeronautics and Astronautics, Nanjing, 210016, China.

Xin Chen is with the Flight Control Research Institute in the College of Automation Engineering, Nanjing University of Aeronautics and Astronautics, Nanjing, 210016, China (corresponding author to provide phone: 025-84892308; e-mail: chenxin@nuaa.edu.cn).

Chuntao Li is with the College of Automation Engineering, Nanjing University of Aeronautics and Astronautics, Nanjing, 210016, China (e-mail: lct115@nuaa.edu.cn).

978-1-4799-4699-0/14/$31.00©2014 IEEE

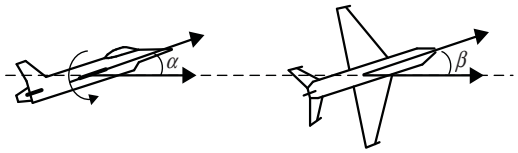

Figure 1. Kinematic coupling

Obviously, a velocity vector roll is desirable from the perspective of eradicating kinematic coupling, but it may unfortunately lead to another debilitating phenomenon 'inertial coupling'. The adverse impaction of such inertial coupling is gyroscopic moment. The inertial coupling is characterized by an aircraft's tendency to align itself perpendicular to rotation vector p_s equals to p_b and r_b during a velocity vector roll, and can have a significant impact on pitching moment M_{ic} (see Fig.2).

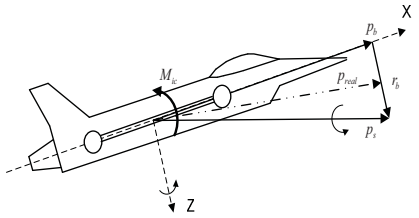

Figure 2. Inertial coupling

B. UAV equations with unmodeled dynamics

Under the assumptions of a flat, non-rotating earth and uniform gravitational field, and all the unmodeled dynamics can be considered in dynamic equations (5), the nonlinear UAV dynamics are modeled by the following equations.

$$\begin{bmatrix}\dot{\beta}\\ \dot{\alpha}\\ \dot{\mu}\end{bmatrix}=\begin{bmatrix}f_\beta\\ f_\alpha\\ f_\mu\end{bmatrix}+\begin{bmatrix}\sin\alpha & 0 & -\cos\alpha\\ -\tan\beta\cos\alpha & 1 & -\tan\beta\sin\alpha\\ \sec\beta\cos\alpha & 0 & \sec\beta\sin\alpha\end{bmatrix}\begin{bmatrix}p\\ q\\ r\end{bmatrix} \tag{1}$$

where

$$f_\beta=\frac{1}{MV}[Y\cos\beta+Mg\cos\gamma\sin\mu-T\sin\beta\cos\alpha] \tag{2}$$

$$f_\alpha=\frac{1}{MV\cos\beta}[Mg\cos\gamma\cos\mu-T\sin\alpha-L] \tag{3}$$

$$f_\mu=\frac{L}{MV}(\sin\mu\tan\gamma+\tan\beta)+\frac{Y}{MV}(\tan\gamma\cos\beta\cos\mu)+\frac{T}{MV}\sin\alpha(\tan\gamma\sin\mu+\tan\beta)$$
$$-\frac{T}{MV}\tan\gamma\cos\mu\cos\alpha\sin\beta-\frac{g}{V}\tan\beta\cos\gamma\cos\mu \tag{4}$$

$$\begin{bmatrix}\dot{p}\\ \dot{q}\\ \dot{r}\end{bmatrix}=\begin{bmatrix}f_p\\ f_q\\ f_r\end{bmatrix}+\begin{bmatrix}c_3 & 0 & c_4\\ 0 & c_7 & 0\\ c_4 & 0 & c_9\end{bmatrix}\begin{bmatrix}\bar{L}\\ M\\ N\end{bmatrix}+\begin{bmatrix}\Delta f_p\\ \Delta f_q\\ \Delta f_r\end{bmatrix} \tag{5}$$

$f_p=(c_1r+c_2p)q$, $f_q=c_5pr-c_6(p^2-r^2)$,

$f_r=(c_8p-c_2r)q$, $c_1=\frac{(I_y-I_z)I_z-I_{xz}^2}{\sum}$, $c_2=\frac{(I_x-I_y+I_z)I_{xz}}{\sum}$,

$c_3=\frac{I_z}{\sum}$, $c_4=\frac{I_{xz}}{\sum}$, $c_5=\frac{I_z-I_x}{I_y}$, $c_6=\frac{I_{xz}}{I_y}$, $c_7=\frac{1}{I_y}$,

$c_8=\frac{I_x(I_x-I_y)+I_{xz}^2}{\sum}$, $c_9=\frac{I_x}{\sum}$, $\sum=I_xI_z-I_{xz}^2$.

Define the state vector of the kinematic equations (1) as $x_1=[\alpha,\beta,\mu]^T$ and that of the dynamic equations (5) as $x_2=[p,q,r]^T$. Then write both the equations (1) and (5) together, we obtain the complete system in the form

$$\begin{cases}\dot{x}_1=f_1(\bar{x}_1)+g_1(x_1)x_2\\ \dot{x}_2=f_2(x_2)+B_nu(t)+\Delta f_2(x_2)\\ y=x_1\end{cases} \tag{6}$$

where $f_1(\bar{x}_1)=[f_\beta,f_\alpha,f_\mu]^T$, $f_2(x_2)=[f_p,f_q,f_r]^T$, and

$$g_1(x_1)=\begin{bmatrix}\sin\alpha & 0 & -\cos\alpha\\ -\tan\beta\cos\alpha & 1 & -\tan\beta\sin\alpha\\ \sec\beta\cos\alpha & 0 & \sec\beta\sin\alpha\end{bmatrix},\ B_n=\begin{bmatrix}c_3 & 0 & c_4\\ 0 & c_7 & 0\\ c_4 & 0 & c_9\end{bmatrix},$$

where $\bar{x}_1=[\alpha,\beta,\mu,\gamma]^T$ is an augmented vector in $f_1(\bar{x}_1)$, $u(t)=[\bar{L},M,N]^T$ is control inputs need to be design . Note that $\Delta f_2(x_2)=[\Delta f_p,\Delta f_q,\Delta f_r]^T$ represents nonlinear uncertain dynamics due to modeling error, aerodynamic coefficient inaccuracy, i.e. roll damping derivatives, and measurement noise.

Control objective: Our goal is to design feedback controller u(t) for plant (6) with unmodeled dynamics such that

- the closed-loop system is stable, that is , all the signals are bounded, and
- the system output y(t) tracks a given reference commands $y_m(t)$ generated by guidance law.

so as to make the UAV turn agilely with smaller sideslip angle especially at high speed, and holding the altitude of vehicle by increasing the angle of attack , to perform rapid turning maneuver.

III. Robust Adaptive Augmented Backstepping Control

In this section, we give the detailed design of the robust adaptive augmented backstepping controller, which consist of a standard backstepping baseline controller [11] and a robust adaptive compensator. To deal with the the couplings of kinematic and inertial, the overall system dynamics (6) can be separated as inner-loop dynamics $(\dot{p},\dot{q},\dot{r})$ and outer-loop dynamics $(\dot{\alpha},\dot{\beta},\dot{\mu})$, and the architecture of the robust adaptive augmented backstepping controller for rapid turning maneuver of UAV is presented in Fig. 3.

A. Backstepping Baseline Controller Design

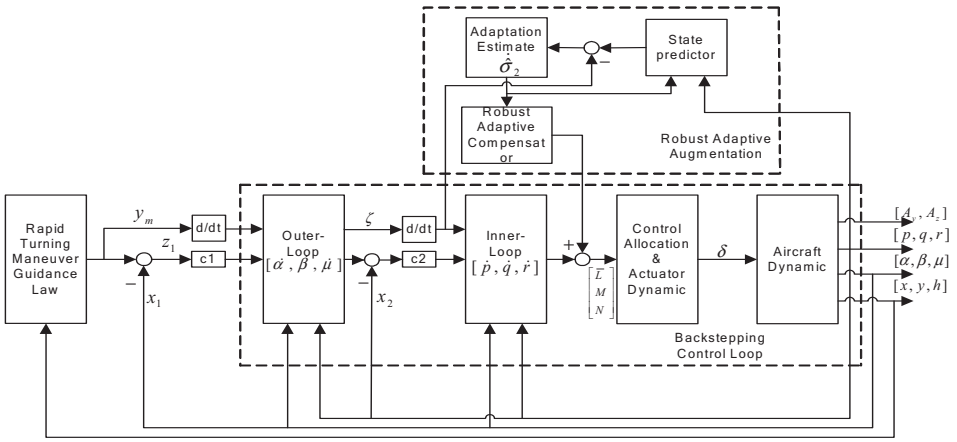

Figure 3. Block diagram of the robust adaptive augmented backstepping control architecture

In (6), state vector x_2 can be considered as the virtual control input of the outer-loop state vector. Then, a desired trajectory of x_2 can be designed using the inner-loop state vector to stabilize the outer-loop state vector and guarantee that $\lim_{t\to\infty}(x_1 - y_m) = 0$. In the following, the control signal $u(t)$ of the global system can be designed using the inner-loop state vector which can guarantee that the inner-loop state vector track the designed desired signal. Such that the outer-loop state vector can track the corresponding reference signal that is the desired system properties can be ensured.

Step 1: Let $z_1 = x_1 - y_m$ and $z_2 = x_2 - \zeta$, where y_m is reference input and ζ is a design function to be determined, from the first equation of (6) we have:

$$\dot{z}_1 = \dot{x}_1 - \dot{y}_m = f_1(\bar{x}_1) + g_1(x_1)(z_2 + \zeta) - \dot{y}_m. \quad (7)$$

To stabilize the first order error system (7), we introduce a Lyapunov function $V_1 = \frac{1}{2} z_1^T z_1$, and the derivative of V_1 is

$$\dot{V}_1 = z_1^T \dot{z}_1 = z_1^T [f_1(\bar{x}) + g_1(x_1)(z_2 + \zeta) - \dot{y}_m]. \quad (8)$$

Choosing $\zeta = g_1^{-1}(x_1)(-c_1 z_1 - f_1(\bar{x}) + \dot{y}_m)$ and $c_1 > 0$, we must note that g1(x1) is nonsingular for all x1, then substitute ζ into (8) we have

$$\dot{V}_1 = z_1^T \dot{z}_1 = -c_1 z_1^T z_1 + z_1^T g_1(x_1) z_2. \quad (9)$$

Hence, if $z_2 = x_2 - \zeta = 0$, we could stabilized the error system (7) using ζ. Since $z_2 \neq 0$, we continue to next step.

Step 2: Construct a new Lyapunov function V_2 as

$$V_2 = V_1 + \frac{1}{2} z_2^T z_2. \quad (10)$$

Considering the second equation of (6), we can obtain the time derivative of V_2 as follows

$$\dot{V}_2 = -c_1 z_1^T z_1 + z_1^T g_1(x_1) z_2 + z_2^T [f_2(x_2) + B_n u + \Delta f_2(x_2) - \dot{\zeta}]. \quad (11)$$

Since $u(t)$ is the actual control input that we have

$$u = u_B - B_n^{-1} \Delta f_2(x_2). \quad (12)$$

with

$$u_B = B_n^{-1}[-f_2(x_2) - c_2 z_2 - g_1(x_1)^T z_1 + \dot{\zeta}] \quad (13)$$

leading to

$$\dot{V}_2 = -c_1 z_1^T z_1 - c_2 z_2^T z_2 \leq 0. \quad (14)$$

Since $\dot{V}_2$ is negative, we have $z_1 \in L_\infty$ and $z_2 \in L_\infty$, the equation (14) implies $z_1 \in L_2$ and from (7) we obtain $\dot{z}_1 \in L_\infty$, using Barbalat's Lemma, we conclude that $\lim_{t\to\infty} z_1(t) = \lim_{t\to\infty}(x_1(t) - y_m(t)) = 0$.

However, since unmodeled dynamics $\Delta f_2(x_2)$ is unknown, the controller $u(t)$ in (12) cannot be obtained accurately, such nonlinear term introduce additional disturbances to the UAV system, which may influence the UAV system's attitude tracking precision, so that the desired asymptotic output tracking performance: $\lim_{t\to\infty}(y(t) - y_m(t)) = 0$ cannot be achieved. Therefore, a robust adaptive control scheme is supposed to be developed to enhance the robustness of control system.

Remark 1. To choose these parameters c_1 and c_2, one has to decide how tight to follow the reference inputs, the physical limitations in real system must be taken into account. And thus it will not be able to track arbitrary fast reference dynamics, so a trade-off between the ability to actually tacking rates on the one hand and desired commands tracking rates on the other hand has to be found. The empirical approach to the problem of selecting a suitable parameter can often be used in practice.

B. Robust Adaptive Compensator Design

To eliminate the effects of unmodeled dynamics on closed-loop system and improve the system performance, an

online state estimator based robust adaptive compensator is developed in this subsection.

Since the moment or product of inertia matrix $B_n \in R^{3\times3}$ in dynamic equations (6) is full rank, then the unmodeled dynamics $\Delta f_2(x_2)$ can be represented as a matched component $B_n\Delta_2(x_2)$ (see [9] and [10]), as a result, the inner-loop dynamics in (6) can be rewritten in the following form

$$\dot{x}_2 = f_2(x_2) + B_n u + B_n\Delta_2(x_2) \tag{15}$$

To design the robust adaptive compensator, the above defined system together with the unmodeled dynamics needs to satisfy the following assumptions.

Assumption 1 The system stare vectors are BIBO stable, i.e., there exist $L_{x1} > 0$ and $L_{x2} > 0$, such that $\|x_2\|_\infty < L_{x2}$.

Assumption 2 For any $\delta > 0$, there exist positive constant B_{d2}, such that $|\Delta_2(x_2)| \le B_{d2}$, for all $\|x_2(t)\|_\infty < \delta$, $\forall t$.

Assumption 3 For any $\delta > 0$, there exist $B_x^\Delta(\delta) > 0$ and $B_t^\Delta(\delta) > 0$, such that for any $\|x_2\|_\infty < \delta$, the partial derivative of $\Delta_2(x_2)$ is piecewise continuous and bounded, i.e., $\left\|\frac{\partial\Delta_2(x_2)}{\partial x_2}\right\| \le B_x^{\Delta 2}(\delta)$, $\left\|\frac{\partial\Delta_2(x_2)}{\partial t}\right\| \le B_t^{\Delta 2}(\delta)$.

State Observer:

$$\dot{\hat{x}}_2 = f_2(x_2) + B_n u + B_n\hat{\sigma}_2(\hat{x}_2) + A_m\tilde{x}_2 \tag{16}$$

with $\hat{x}_2(0) = x_2(0)$, where $\hat{x}_2 \in R^3$ is the virtual estimator state and $\tilde{x}_2 = \hat{x}_2 - x_2$ is the estimator state error vector, $A_m \in R^{3\times3}$ is any Hurwitz matrix. Given arbitrary symmetric matrix $Q > 0$, there exists a symmetric matrix $P > 0$, satisfies $PA_m + A_m{}^T P = -Q$. $\hat{\sigma}_2(\hat{x}_2)$ is the estimator of unmodeled dynamics $\Delta_2(x_2)$.

Control Law:

The developed robust adaptive controller structure incorporates backstepping feedback control law $u_B(t)$ and an adaptive state observe-based feedforward compensator $u_{ad}(t)$, which are expressed as:

$$u(t) = u_B(t) + u_{ad}(t), \tag{17}$$

$$u_{ad}(t) = -B_n{}^{-1}\hat{\sigma}_2(\hat{x}_2). \tag{18}$$

Robust adaptive Laws:

$$\dot{\hat{\sigma}}_2(\hat{x}_2) = \Gamma\,\mathrm{Pr}oj(\hat{\sigma}_2, -B_n{}^T P\tilde{x}_2),\ \hat{\sigma}_2(\hat{x}_2(0)) = 0 \tag{19}$$

where $\Gamma \in R^+$ are the adaptation gain matrix, $\mathrm{Pr}oj$ is projection-based operator which ensures the boundness of $\|\hat{\sigma}_2\|$.

C. Performance Analysis

The detailed analysis of the stability of closed-loop system is given in this subsection, which indicates that the overall system is uniformly asymptotic stable and the tracking error gradually converges to a bounded region under the Assumptions 1-3.

Denote $\tilde{x}_2 = \hat{x}_2 - x_2$ and $\tilde{\sigma}_2 = \hat{\sigma}_2 - \Delta_2$, we first proof the boundedness of $\tilde{x}_2$ and $\tilde{\sigma}_2$. From equation (15) and equation (16), we have [12]

$$\dot{\tilde{x}}_2 = B_n\tilde{\sigma}_1(t) + B_m\tilde{\sigma}_2(t) + A_m\tilde{x}_2, \tag{20}$$

chose a Lyapunov function candidate

$$V(\tilde{x}_2, \tilde{\sigma}_1, \tilde{\sigma}_2) = \tilde{x}_2^T P\tilde{x}_2 + \tilde{\sigma}_2^T\Gamma^{-1}\tilde{\sigma}_2. \tag{21}$$

where $P \in R^{3\times3}$ is a positive definite symmetric matrix that satisfies $PA_m + A_m{}^T P = -Q$, for a chosen matrix $Q = Q^T > 0$. Computing the time derivative of $V(\tilde{x}_2, \tilde{\sigma}_2)$, we obtain

$$\dot{V} = -\tilde{x}_2^T Q\tilde{x}_2 + 2\tilde{x}_2^T PB_n\tilde{\sigma}_2 + 2\tilde{\sigma}_2^T\Gamma^{-1}\dot{\hat{\sigma}}_2 - 2\tilde{\sigma}_2^T\Gamma^{-1}\dot{\Delta}_2 \tag{22}$$

The projection adaptation law (19) ensures [13] [14]

$$\tilde{x}_2^T PB_n\tilde{\sigma}_2 + \tilde{\sigma}_2^T\Gamma^{-1}\dot{\hat{\sigma}}_2 \le 0 \tag{23}$$

which leads to

$$\dot{V} \le -\tilde{x}_2^T Q\tilde{x}_2 - 2\tilde{\sigma}_2^T\Gamma^{-1}\dot{\Delta}_2. \tag{24}$$

In what follows, we proof the following statement using contradiction.

$$V(\tau) \le \eta,\ \forall\tau \in [0, t) \tag{25}$$

where

$$\eta = 4\frac{\lambda_{max}(P)}{\lambda_{\min}(Q)} I_{n\times n}(B_{d2}\Gamma^{-1}B_t^{\Delta 2}) + 4\Gamma^{-1}B_{d2}^2,$$

and $B_t^{\Delta 2}$, B_{d1} are defined in Assumptions 2-3.

Then, if at any time $t' \in [0, t)$, $\exists V(t') > \eta$, it follows from (21) that

$$V(t') = \tilde{x}_2^T P\tilde{x}_2 + \tilde{\sigma}_2^T\Gamma^{-1}\tilde{\sigma}_2 > \eta. \tag{26}$$

Then we have

$$\tilde{x}_2^T P\tilde{x}_2 > 4\frac{\lambda_{max}(P)}{\lambda_{\min}(Q)} B_{d2}\Gamma^{-1}B_t^{\Delta 2}. \tag{27}$$

Therefore

$$\tilde{x}_2^T Q\tilde{x}_2 > 4B_{d2}\Gamma^{-1}B_t^{\Delta 2}, \tag{28}$$

which implies that $\dot{V}(t') < 0$, $t' \in [0, t)$, since that

$$V(0) = \|\hat{\sigma}_2(0) - \Delta_2(x_2(0))\|^2\,\Gamma^{-1} < \eta. \tag{29}$$

It follows that $V(\tau) \le \eta$, $\forall\tau \in [0, t)$, which yields

$$\|\tilde{\sigma}_2(x_2)\|_\infty \in L_\infty, \text{ and } \|\tilde{x}_2(\tau)\|_\infty \in L_\infty,\ \forall\tau \in [0, t). \tag{30}$$

Next, rewriting $\dot{V}_2$ in (11) as

$$\dot{V}_2 = -c_1 z_1^T z_1 + z_1^T g_1(x_1) z_2 + z_2^T [f_2(x_2) + B_n u_B(t) + B_n \tilde{\sigma}_2(t) - \dot{\zeta}]. \quad (31)$$

Using $u_B(t) = B_n^{-1}[-f_2(x_2) - c_2 z_2 - g_1(x_1)^T z_1 + \dot{\zeta}]$ and (30), from Young's Inequality,

$$(z_2^T)(B_n \tilde{\sigma}_2(t)) \le \varepsilon \|z_2\|^2 + \eta_n^2 / 4\varepsilon,$$

where η_n denotes the upper bound of $B_n \tilde{\sigma}_2(t)$, we have

$$\dot{V}_2 \le -cV_2 + \eta_n^2 / 2\varepsilon. \quad (32)$$

where $c = \min\{2c_1, 2(c_2 - 2)\}$.

If $V_2 = \varphi$ and $c > \eta_n^2 / 2\varepsilon\varphi$, then we have $\dot{V}_2 < 0$, that is, if $V_2(0) < \varphi$, then $V_2(t) \le \varphi$. Solving (32), we can obtain that

$$0 \le V_2(t) < \eta_n^2 / 2\varepsilon\varphi + [V_2(0) - \eta_n^2 / 2\varepsilon\varphi] e^{-ct}, \quad (33)$$

so that z_1 and z_2 are uniformly ultimately bounded. Furthermore, the (33) gives that

$$\lim_{t \to \infty} sup\, V_2(t) \le \eta_n^2 / 2\varepsilon\varphi, \quad (34)$$

which implies the tracking error $z_1 = x_1 - y_m$ can converge to a sufficiently small residual set. So that the desired control objective is met.

IV. Simulation Study

In this section, a serious of simulation is made on a high agility UAV model with small aspect ratio and high thrust-to-weight ratio in the full flight envelop. The aerodynamic data are valid up to 0.5 Mach, angle of attack range of $-10° \le \alpha \le 50°$, sideslip angle range of $-30° \le \beta \le 30°$. And the intermediate points of aerodynamic data are linearly interpolated. Besides, a normal daisy chain control allocation algorithm, which serves as a map from moments to deflection of rudders, is used in the simulations.

A. Simulation Results of rapid turning maneuver in full envelop

The rapid turning maneuver commence with horizontal flight at a particular speed and altitude. The UAV tracks the commands generated by guidance law to turn with about 250m turning radius while holding the initial altitude. The control parameters c_1 and c_2, as well as the adaptation gain matrix Γ are selected and presented in TableC. And the entire closed-loop control system is simulated at the original sampling rate of 200 Hz.

TABLE I. Control Parameters and Adaptive Gain

Flight Envelop Points	C_1	C_2	Γ
Alt=3000m V=120m/s	[4,6,4]	[9,13,9]	diag{10,4,2}
Alt=1500m V=90m/s	[3,5,3]	[6,11,6]	diag{8,3,2}
Alt=500m V=60m/s	[1,3,1]	[3,7,3]	diag{5,2,2}

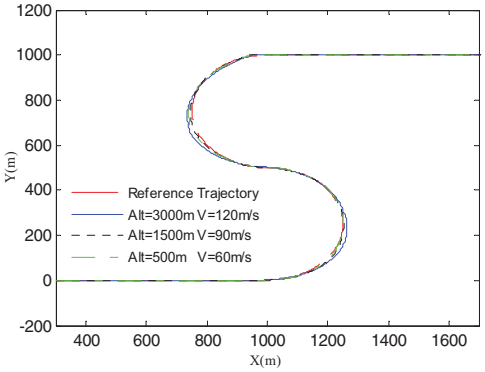

Figure 4 Rapid turning in different envelop points

As shown in Fig.4, the UAV is able to perform rapid turning maneuver in full flight envelop successfully. The bank angel reaches 78° during turning to generate large centrifugal force for aircraft to turn agilely especially at the speed of 120 m/s. As displayed in Fig.5, the bank angle about the velocity reaches 67°and the average time to accomplish the maneuver is 25s, which represent the high agility of the UAV. Since the big bank angle leads to the decrease of lift, the vehicle needs to increase the angle of attack to compensate the loss of lift to maintain a constant altitude while holding the airspeed at the initial value.

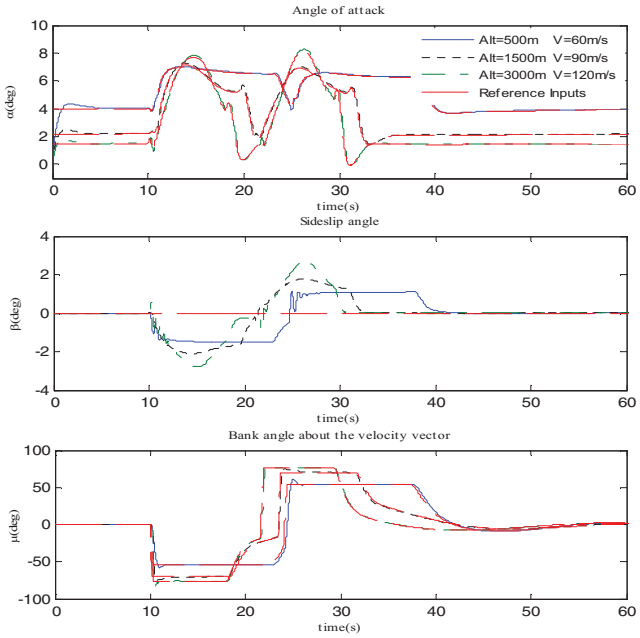

Figure 5 Outer-loop states response in different envelop regions

B. Simulations of Robustness Validation

To assess the effectiveness and robustness of the proposed control scheme, the deviations of aerodynamic damping coefficients given in Table Ⅱ are introduced in the UAV nonlinear model. The contrastive simulation results of inner-loop response and the three-axis adaptive compensation moment vector $\hat{\sigma}_2(\hat{x}_2)$ are presented in Fig.7.

TABLE II. Deviation of Aerodynamic Damping Cofficients

Aerodynamic Coefficients	C_{lp}	C_{lr}	C_{mq}	C_{nq}	C_{nq}

Aerodynamic Coefficients	C_{lp}	C_{lr}	C_{mq}	C_{nq}	C_{nq}
Deviation Range	20%	30%	-50%	-30%	20%

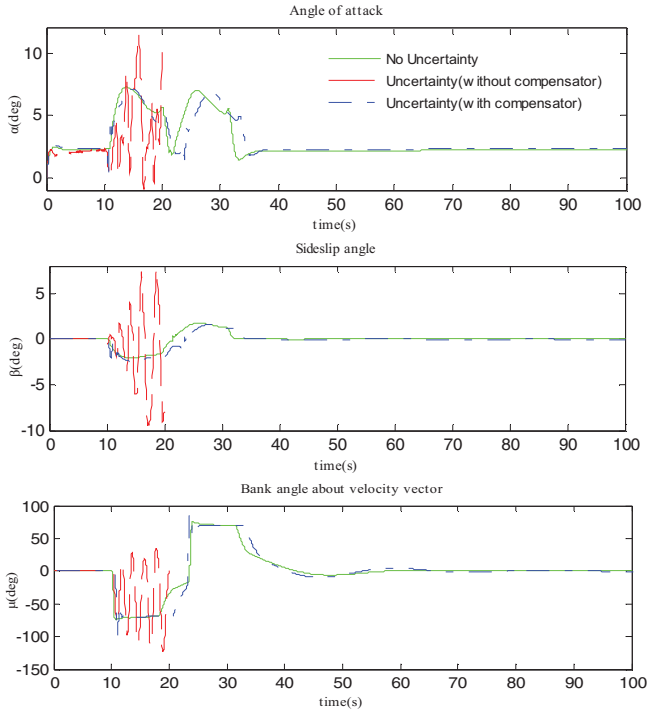

Figure 6 Outer-loop states response with and without compensator

As expected, the controller is trying to minimize the state error $\tilde{x}_2 = \hat{x}_2 - x_2$. However, the control system without compensator has become unstable after adding uncertain dynamics in the UAV model revealed in Fig.6. While the proposed control scheme with robust adaptive compensator in the paper successfully perform the maneuver in the presence of unmodeled dynamics. The contribution made by the adaptive compensation roll moment L_{ad} is more notable in the maneuver, since it counteracts the adverse effect caused by changes of rolling damp coefficient in the fast rolling behavior displayed in Fig.7.

ACKNOWLEDGMENT

This work was supported by Science and Technology on Aircraft Control Laboratory under grant 20125852057. And Funding of Jiangsu Innovation Program for Graduate Education under grants CXLX12_0159 and the Fundamental Research Funds for the Central Universities.

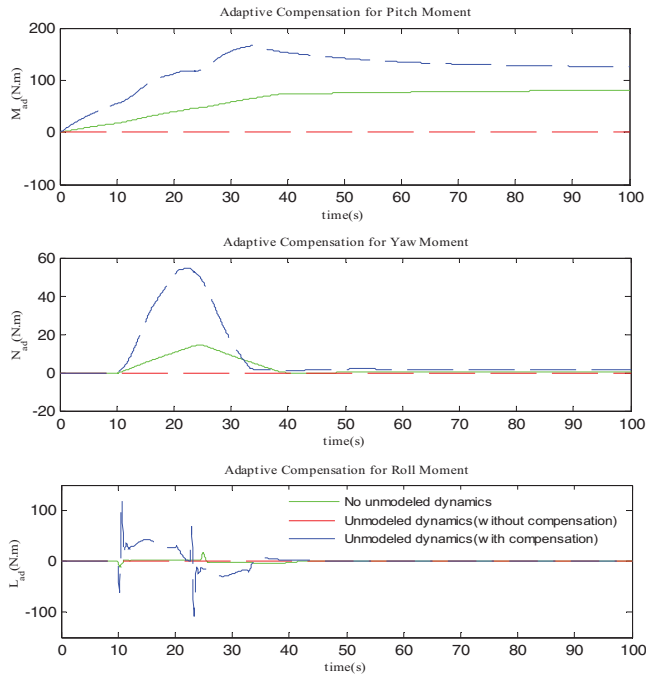

Figure 7 Adaptive compensation moments

REFERENCES

[1] W. Schneider, "Defense science board study on unmanned aerial vehicles and uninhabited combat aerial vehicle." *Department of defense Tech. Rep.* http://www.iwar.org.uk/ram/resources/dsb/uav.pdf

[2] C. W. Alcorn, M. A. Croom, M. S. Francis and H. Ross, "The X-31 aircraft: advances in aircraft agility and performance," *Prog, Aerospace Sci*, 1996, pp. 377–413

[3] A. Frank, J. McGrew, M. Valenti, D. Levine and J. How, "Hover, transition, and level flight control design for a single-propeller indoor airplane," *AIAA Guidance, Navigation, and Control Conference and Exhibit,* August 2007,pp. 249-273.

[4] S. Antony Snell, Dale F. Enns and William L, "Garrard Jr. Nonlinear inversion flight control for a super-maneuverable aircraft," *Journal of Guidance, Control, And Dynamics,* 15(4), pp. 1121-1139, Aug 1992.

[5] N. Kemal and Gokhan Inalhan, "Autonomous control of unmanned combat air vehicles: design of a multimodal control and flight planning framework for agile maneuvering," *IEEE control systems magazine*, pp. 74-95, October, 2012.

[6] M. M. Polycarpou and P. A. Ioannou, "A robust adaptive nonlinear control design," *Automatic.*, 32(3), pp. 423-427, 1996.

[7] L. Sonneveldt, Q. P. Chu and J. A. Muler, "Nonlinear flight control design using constrained adaptive backstepping," *Journal of Guidance, Control, and Dynamics.*, 30(2), pp. 549-573, March-April, 2007.

[8] M. McFarland and A. J. Calise, "Robust adaptive control of uncertain nonlinear systems using neural networks," *American Control Conference,* Albuquerque, NM, June, 1997.

[9] Enric Xargay, Naira Hovakimyan, and Chengyu Cao, "L1 Adaptive output feedback controller for nonlinear systems in the presence of unmodeled dynamics," *Proceedings of American Control Conference*, Hyatt Regency Riverfront, St. Louis, pp. 947-965, June 10-12, 2009.

[10] Xiaofeng Wang, Naira Hovakimyan, "L1 adaptive controller for nonlinear time-varying reference systems," *System & Control Letters*, vol. 61, pp. 455-463, 2012.

[11] M. Krsti´c, I. Kanellakopoulos and P. V. Kokotovi´ c, *Nonlinear and adaptive control design*. New York: Wiley, 1995.

[12] Tyler Leman, Enric Xargay, Geir Dullerud, Naira Hovakimyan, "L1 adaptive control augmentation system for the X-48B aircraft," *AIAA Guidance, Navigation, and Control Conference,* Chicago, Illinois, pp. 10-13, August 2009.

[13] M. Annaswamy, E. Lavretsky, T. Dydek, E. Gibson and M. Matsutani, "Recent results in robust adaptive flight control systems," Int.J. Adapt. Control Signal Process. 27, pp. 4-21, 2013.